Progress In Electromagnetics Research, Vol. 116, 271–296, 2011

COMPRESSION AND RADIATION OF HIGH-POWER SHORT RF PULSES. II. A NOVEL ANTENNA ARRAY DESIGN WITH COMBINED COMPRESSOR/RADIATOR ELEMENTS

K. Sirenko

King Abdullah University of Science and Technology (KAUST)
4700 KAUST, Thuwal, 23955-6900, Saudi Arabia

V. Pazynin and Y. Sirenko

Institute of Radiophysics and Electronics of National Academy of Sciences of Ukraine (IRE NASU)
12 Acad. Proskura Str., Kharkiv, 61085, Ukraine

H. Bağci

King Abdullah University of Science and Technology (KAUST)
4700 KAUST, Thuwal, 23955-6900, Saudi Arabia

Abstract—The paper discusses the radiation of compressed high power short RF pulses using two different types of antennas: (i) A simple monopole antenna and (ii) a novel array design, where each of the elements is constructed by combining a compressor and a radiator. The studies on the monopole antenna demonstrate the possibility of a high power short RF pulse's efficient radiation even using simple antennas. The studies on the novel array design demonstrate that a reduced size array with lower pulse distortion and power decay can be constructed by assembling the array from elements each of which integrates a compressor and a radiator. This design idea can be used with any type of antenna array; in this work it is applied to a phased array.

Received 20 February 2011, Accepted 26 April 2011, Scheduled 4 May 2011
Corresponding author: Kostyantyn Sirenko (kostyantyn.sirenko@kaust.edu.sa).

1. INTRODUCTION

Almost any paper on microwave energy compression focuses just on the design of compressors as a whole [1, 2] or their (isolated) components [3, 4], the generation of compressed pulses [5, 6], or, rarely, the details of the energy accumulation processes — see Part I of this paper). However, the design of the compressors and the generation of the high-power compressed short pulses are only one half of the story. For most of the applications, the output port of the compressor is either connected to a waveguide to be transmitted to a load [7, 8] or to an antenna to be radiated [9, 10]. Transmission of the compressed pulses on waveguides is rather straightforward to study and understand. However, the topic of radiation of compressed pulses is practically untouched. This paper is intended to fill up this gap.

The output of a microwave compressor is a high-power short RF pulse [1]. The bandwidth of compressed pulse is determined by the spectral composition of the excitation (input) pulse and the energy accumulation and exhaust processes that take place in the compressor. Since the compressor is a resonant device, the bandwidth of compressed (output) pulse is never wide. No specially designed antenna is required to efficiently radiate the compressed pulse; in the other words one can use even rather simple antennas [11–14] to distribute compressed pulse's energy in space and time with low distortion and loss. This obviously means that depending on the specific application, one may prefer to use a complicated antenna or array of antennas.

The contributions of this paper are twofold: (i) It studies the radiation of a short RF pulse from monopole antenna mounted on a ground plane. The purpose of this study is to demonstrate that the compressed pulses can efficiently be radiated using simple antennas. (ii) It presents a novel array design, where each of the array elements is constructed by combining a compressor and a radiator. The proposed design allows to eliminate the waveguide between compressor and radiator and, thus, reduces the overall size and the weight of the array. It also reduces the distortion in the pulse and absorption loss since the overall distance covered by pulse in lossy and dispersive waveguides is reduced. Additionally, the proposed design has the advantage of compressing the pulse right before it is radiated, allowing the use of components with low handling power in the rest of the array. In this work, this novel design idea is applied to a phased antenna array; the "improved" phased antenna array is intended for generation and directional radiation of high-power short pulses and shares the most significant advantage of "common" phased arrays, viz. rapid electronic beam steering without the movement of the array itself.

The remainder of the paper is organized as follows. Section 2 introduces the mathematical model and antenna characteristics that are referred to in the subsequent studies. Section 3 discusses the use of a simple monopole antenna for radiating compressed pulses. Section 4 presents the novel design, where each of the array elements is constructed by combining a compressor and a radiator, and details its application to a phased array. Section 5 presents conclusions and future research avenues.

It should be noted here that the microwave compressors utilized in this work are designed using the scheme detailed in the first part of this paper. The simulations used in the designs and the characterization of antennas are performed using the finite difference time domain (FDTD) scheme with FFT-accelerated exact absorbing boundary conditions (EACs), which is briefly described in [17] and formulated in great detail in [15].

2. MATHEMATICAL MODEL AND CHARACTERISTICS OF ANTENNAS

This section first introduces the mathematical model in Section 2.1 and then describes, in Section 2.2, the fundamental antenna characteristics in terms of mathematical model parameters, which are referred to in the subsequent sections, Sections 3 and 4, to detail the radiation of the compressed pulses.

2.1. Mathematical Model

Consider an example axially-symmetric radiating antenna presented in Fig. 1. Electromagnetic wave interactions on this structure are mathematically modelled by the following initial-boundary value problem [15]:

$$\begin{aligned}
&\left[-\varepsilon_r(g)\partial_t^2 - P + \partial_z^2 + \partial_\rho\left(\rho^{-1}\partial_\rho\rho\right)\right] U(g,t) = 0; \quad t>0, \quad g=\{\rho,z\}\in\mathbf{Q}\\
&U(g,0)=0, \quad \partial_t U(g,t)|_{t=0} = 0; \quad g\in\overline{\mathbf{Q}}_L\\
&E_{tg}(g,t)|_{p=\{\rho,\phi,z\}\in\mathbf{S}} = 0,\ U(0,z,t) = 0; \quad t\geq 0
\end{aligned} \tag{1}$$

Here, $\{\rho,\phi,z\}$ and $\{r,\phi,\theta\}$ represent the cylindrical and spherical coordinate systems; $U = E_\phi$, $E_\rho = E_z = H_\phi = 0$, $P[U] = \partial_t[Z_0\sigma_0(g,t)U(g,t)]$ for $TE_{0,n}$ waves and $U = H_\phi$, $H_\rho = H_z = E_\phi = 0$, $P[U] = Z_0\sigma_0(g,t)\partial_t U(g,t)$ for $TM_{0,n}$ waves; $\vec{E}(g,t) = \{E_\rho, E_\phi, E_z\}$ and $\vec{H}(g,t) = \{H_\rho, H_\phi, H_z\}$ are the vectors of electric and magnetic fields; $\mathbf{S}$ represents the surface of perfect electrically conducting (PEC)

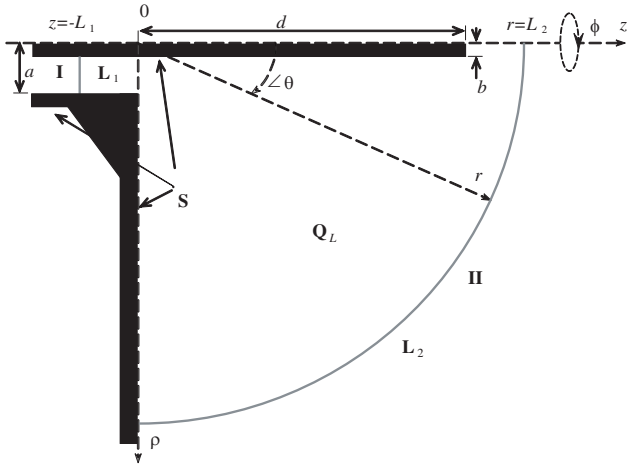

Figure 1. Geometry of the model monopole radiator.

parts of the antenna; $E_{tg}(g,t)$ is the component of the electric field that is tangential to $\mathbf{S}$; $\mathbf{Q} = \mathbf{Q}_L \cup \mathbf{I} \cup \mathbf{II} \cup \mathbf{L_1} \cup \mathbf{L_2}$ is the physical domain — it is a part of the half-plane $\phi = \text{const}$ which is bounded by $\mathbf{S}$; $\mathbf{Q}_L \in \mathbf{Q}$ is the computation domain — it is a part of $\mathbf{Q}$ which is bounded by the virtual boundaries $\mathbf{L}_1$ and $\mathbf{L}_2$; $\sigma_0(g,t)$ and $\varepsilon_r(g)$ represent the conductivity and the relative permittivity; $Z_0 = (\mu_0/\varepsilon_0)^{1/2}$, ε_0 and μ_0 are the wave impedance, permittivity and permeability of the free space, respectively. $\sigma_0(g,t)$ and $\varepsilon_r(g)$ are piecewise constant functions in space and the conductivity's time dependence is utilized to simulate changes in the compressor's mode of operation. Domains $\mathbf{I} = \{g = \{\rho, z\} \in \mathbf{Q} : \ b \le \rho \le a, \ z < -L_1\}$ and $\mathbf{II} = \{g = \{r, \vartheta\} \in \mathbf{Q} : \ r > L_2\}$ represent infinite regular input (feeding) circular ($b = 0$) or coaxial ($b > 0$) waveguide and homogeneous external region, respectively. Contours $\mathbf{L}_1 = \{g = \{\rho, z\} \in \mathbf{Q} : \ z = -L_1\}$ and $\mathbf{L}_2 = \{g = \{r, \vartheta\} \in \mathbf{Q} : \ r = L_2\}$ represent virtual boundaries between $\mathbf{I}$ and $\mathbf{II}$ and the computation domain $\mathbf{Q}_L$, respectively. The physical domain $\mathbf{Q}$ is unbounded in the r direction at the radiating end and in the z direction at the feeding end. In this formulation, the SI system is used for all physical quantities except the time t, which is multiplied with the speed of light in free space and measured in meters.

Let $U^i(g,t)$ represent an incident pulse (excitation), which arrives from the feeding waveguide $\mathbf{I}$ upon the virtual boundary $\mathbf{L_1}$ at time $t > 0$. The total field $U(g,t)$ in $\mathbf{I}$ can be represented as a sum of incident and scattered fields: $U(g,t) = U^i(g,t) + U_1^s(g,t)$, $g = \{\rho, z\} \in \mathbf{I}$; the total field in $\mathbf{II}$ consists of only the scattered field: $U(g,t) = U_2^s(g,t)$,

$g = \{r, \vartheta\} \in \mathbf{II}$. $U^i(g,t)$, $U_1^s(g,t)$, and $U_2^s(g,t)$ are represented in terms of modes via separation of variables [15]:

$$\begin{aligned} U_1^s(g,t) &= \sum_n u_{n,1}(z,t)\ \mu_{n,1}(\rho), \\ U^i(g,t) &= \sum_n v_{n,1}(z,t)\,\mu_{n,1}(\rho); \quad g = \{\rho, z\} \in \mathbf{I}, \\ U_2^s(g,t) &= \sum_n u_{n,2}(r,t)\ \mu_{n,2}(\cos\vartheta); \quad g = \{r, \vartheta\} \in \mathbf{II}. \end{aligned} \tag{2}$$

The spatio-temporal (mode) amplitudes $v_{n,1}$ and $u_{n,j}$, and the transverse functions $\mu_{n,j}$, $j = 1, 2$ are related by

$$\left\{ \begin{array}{c} u_{n,1}(z,t) \\ v_{n,1}(z,t) \end{array} \right\} = \int_b^a \left\{ \begin{array}{c} U_1^s(g,t) \\ U^i(g,t) \end{array} \right\} \mu_{n,1}(\rho)\,\rho d\rho; \quad g = \{\rho, z\} \in \mathbf{I},$$

$$u_{n,2}(r,t) = \int_0^{\pi/2} U(g,t)\,\mu_{n,2}(\cos\vartheta)\sin\vartheta d\vartheta; \quad g = \{r, \vartheta\} \in \mathbf{II}.$$

Here, $a > 0$ and $b \geq 0$ represent the outer and inner radiuses of the waveguide $\mathbf{I}$ (see Fig. 1). It should be noted that $v_{n,1}$, $u_{n,j}$ and $\mu_{n,j}$, $j = 1, 2$ define a complete set of modes for representing the waves $U^i(g,t)$ and $U_j^s(g,t)$. The transverse functions $\mu_{n,j}$ and the corresponding eigenvalues $\lambda_{n,j}$ are known and can be found in [15] and are not repeated here.

The unbounded (open) problem (1) in the domain $\mathbf{Q}$ can be converted into a bounded (closed) one in the domain $\mathbf{Q}_L$, suitable for numerical discretization and solution, by introducing EACs on the virtual boundaries $\mathbf{L}_1$ and $\mathbf{L}_2$ (Fig. 1). In this work, the EACs derived in [15] are used. It should be noted here that enforcing EACs on virtual boundaries results in mathematically exact conversion of the unbounded problem to the bounded one. The EACs on the virtual boundaries $\mathbf{L_1}$ and $\mathbf{L_2}$ are [15]:

$$\begin{aligned} & U(\rho, -L_1, t) - U^i(\rho, -L_1, t) \\ = & \sum_n \left\{ \int_0^t J_0\left[\lambda_{n,1}\ (t-\tau)\right] \left[\int_{b_1}^{a_1} \partial_z \left[U(\tilde{\rho}, z, \tau) - U^i(\tilde{\rho}, z, \tau) \right] \right|_{z=-L_1} \right. \\ & \left. \times \mu_{n,1}(\tilde{\rho})\,\tilde{\rho} d\tilde{\rho} \right] d\tau \Big\} \mu_{n,1}(\rho); \quad b_1 \leq \rho \leq a_1, \quad t \geq 0, \end{aligned}$$

$$
\begin{aligned}
& U\left(r,\vartheta,t\right) \\
&= \sum_n \left\{ \left(\frac{L_2}{r}\right)^{n+1} \int_0^{\pi/2} U\left(L_2,\tilde{\vartheta},t-(r-L_2)\right)\mu_{n,2}\left(\cos\tilde{\vartheta}\right)\sin\tilde{\vartheta}d\tilde{\vartheta} \right. \\
&\quad + \sqrt{\frac{L_2}{r}} \int_0^{t-(r-L_2)} S_{n+1/2}(r,L_2,t-\tau) \\
&\quad \left. \times \left[\int_0^{\pi/2} \partial_\tau U(L_2,\tilde{\vartheta},\tau)\mu_{n,2}(\cos\tilde{\vartheta})\sin\tilde{\vartheta}d\tilde{\vartheta} \right] d\tau \right\} \mu_{n,2}(\cos\theta); \\
& g=\{r,\vartheta\}\in \mathbf{II}, \quad t\geq 0.
\end{aligned}
$$

Here, $J_0(\cdot)$ represents the Bessel function of the zeroth order,

$$
S_\gamma\left(r,L_2,t-\tau\right)=\sum_s \frac{H_\gamma^{(1)}\left(z_s r\right)}{H_{\gamma-1}^{(1)}\left(z_s L_2\right)} \frac{\exp\left[-iz_s\left(t-\tau\right)\right]}{z_s L_2},
$$

z_s are zeros of the Hankel function of the first kind, $H_\gamma^{(1)}(zL_2)$, and index s runs through all of them (there are only finite number of these zeros). Although the EAC for the boundary $\mathbf{L_2}$ is derived in spherical coordinates $\{r,\vartheta\}$, it is meant for implementation in cylindrical coordinates $\{\rho,z\}$. It should be noted here that these EACs are nonlocal both in space and time (note the ranges of integrals over τ and $\tilde{\rho}$); their direct numerical implementation results in increased computational requirements. This can be alleviated by using localization techniques [15–17] or by accelerating the computation of temporal convolutions via the use of blocked FFTs [18–24] as described in [15]. Both of these techniques are exact, i.e., their application does not introduce additional errors into the numerical solution. Details on the discretization and the numerical implementation of the EACs and the localization and the FFT-based acceleration can be found in [15].

Problem (1) supplemented with the EACs on the virtual boundaries $\mathbf{L}_1$ and $\mathbf{L}_2$ is solved numerically using the FDTD method described in [15]. The numerical solution provides the near-field distribution of electromagnetic waves in the computation domain $\mathbf{Q}_L$. In the far-field region, where the angular field distribution is essentially independent of the distance from the antenna [14], the field distribution is obtained using the transport operator, which allows for computation of the field values on any arc $r=M>L_2$ from the field values on the

boundary $\mathbf{L}_2$ ($r = L_2$) [15–17]. Thus, knowing the field distribution in the near-field region (or, i.e., in the computation domain $\mathbf{Q}_L$), one can obtain all standard antenna characteristics [14].

2.2. Characteristics of Antennas

Several fundamental antenna characteristics, which are used in the explanation of the compressed pulses' radiation in Sections 3 and 4, are briefly reviewed here:

(i) *Normalized power pattern* characterizes the distribution of the radiated field's power as a function of space and frequency. The normalized power pattern is computed in the far-field region of the antenna on the arc $r = M \geq L_2$ and is defined as

$$D(M, \vartheta, k) = \left(\frac{\left| \tilde{E}_{tg}(M, \vartheta, k) \right|}{\max\limits_{0<\vartheta<\pi/2} \left| \tilde{E}_{tg}(M, \vartheta, k) \right|} \right)^2. \tag{3}$$

Here, $0 \leq \vartheta \leq 90^\circ$ is an elevation angle, which is measured in degrees from the z axis (see Fig. 1), $k = 2\pi/\lambda$ is the wavenumber, λ is the wavelength, $\tilde{E}_{tg}$ is the component of the (frequency-domain) electric field tangential to line of the arc and is obtained by Fourier transforming time-domain electric field E_{tg} computed from the numerical solution of (1). In this work, a normalized power pattern definition that depends on space and frequency is preferred over the conventional one, which only depends on space and is evaluated at discrete frequencies [14], not because it is very easily obtained from time domain simulations with no extra cost, but also it allows for easy and accurate detection of frequency dependent changes in the power distribution. $D(M, \vartheta, k)$ can be used to determine if all the frequency components contained in a pulse propagate in the same direction or "prefer" different ones causing the scattering of the pulse in different directions.

(ii) *Direction of the main beam* is represented by $\bar{\vartheta}(k)$ and is the angle, along which the maximum radiation occurs, i.e., $D(M, \bar{\vartheta}(k), k) = 1$.

(iii) *Half-power beamwidth HPBW* is represented by $\vartheta_{0.5}(k)$ and is the angular separation between two angles of the main beam, where the maximum power reduces to the half of its maximum value, i.e. $\vartheta_{0.5}(k) = |\vartheta^+ - \vartheta^-|$, where $D(M, \vartheta^+, k) = 0.5$ and $D(M, \vartheta^-, k) = 0.5$.

(iv) *Normalized pulse pattern* characterizes the distribution of the field as a function of space and time. The normalized pulse pattern

is computed in the far-field region of the antenna on the arc $r = M \geq L_2$ and is defined as

$$D_P(M, \vartheta, t) = \frac{U(M, \vartheta, t)}{\max\limits_{\vartheta, t} |U(M, \vartheta, t)|}. \tag{4}$$

Here, $U(M, \vartheta, t)$ represents one of the field components, for example, it represent the ϕ component for axially symmetric structures (see (1)), or the x component for 2-D structures, (see (1) in the first part of this paper). This characteristic allows for characterizing spatial (angular) and temporal distribution of the radiated pulse on a given distance from the source. It provides a measure to evaluate if a pulse is localized and preserves it shape or scatters as it propagates away from the source; different parts of the pulse, such as forerunner or tail, may "prefer" different directions. Similar to the normalized power pattern, it is possible to define the direction of the main lobe, $\bar{\vartheta}_P$, (it is direction where $|D_P(M, \vartheta, t)|$ reaches it maximum) and, correspondingly, the half-power beamwidth, $\vartheta_P^{0.5}$.

(v) *Frequency-domain radiation efficiency* is the ratio of the energy radiated by the antenna into the free space to the total input energy at a given frequency. In the case of no loss in the structure (i.e., under the assumption of PEC walls) and excitation by the pth propagating mode from the feeding waveguide **I**, the frequency-domain radiation efficiency is defined as

$$\eta_{fr}(k) = 1 - \sum_n W_{p,n}^R(k). \tag{5}$$

Here, $W_{p,n}^R(k)$ is the relative part of energy reflected into nth mode of the waveguide **I**, see Section 2.3 in Part I for details. It should be noted here that in (5), the power loss due to mismatch of the power generator and the feeding waveguide is not taken into account.

For antenna arrays, the frequency-domain efficiency is generalized as

$$\eta_{fr,arr}(k) = \sum_i \left(1 - \sum_{j,n} W_{p,n}^{i,j}(k)\right) \Big/ N.$$

where N is the total number of feeding waveguides, $W_{p,n}^{i,j}(k)$ is the relative part of energy reflected back into the nth mode of the jth waveguide when the array is excited by the pth mode of the ith waveguide, and the summation is performed over all modes (index n) in all waveguides (index $j = 1, 2, \ldots, N$) for all feeding waveguides (index $i = 1, 2, \ldots, N$).

(vi) *Time-domain radiation efficiency* is a ratio of the energy radiated by the antenna into the free space to the total input energy and is defined as

$$\xi = \frac{W_1^i(0;T) - W_1^s(0;T)}{W_1^i(0;T)}. \tag{6}$$

Here, T is the end of the observation duration, $W_1^s(0;T)$ represents the energy reflected back into the feeding waveguide **I**, and $W_1^i(0;T)$ represents the total input energy. $W_1^s(0;T)$ and $W_1^i(0;T)$ are computed from the integrals of the corresponding instantaneous powers, see Section 2.2 in Part I for details. According to the law of energy conservation, in the absence of loss the difference between the total input energy, $W_1^i(0;t)$, and the one reflected back into the feeding waveguide, $W_1^s(0;t)$, is equal to the radiated energy.

3. RADIATION OF COMPRESSED PULSES BY SIMPLE ANTENNAS

Because of the resonant nature of the energy accumulation and exhaust processes inside the compressor, the bandwidth of the compressed output pulse is rather narrow. This means that simple antennas can efficiently be used for radiating compressed pulses. Most of these antennas operate efficiently in a narrow band of frequency, which can be shifted by simple modifications to their geometry (e.g., changing the length of the monopole). Because of this simplicity, if the application requirements are not strict, these antennas can be preferred for radiating short compressed pulses.

In this section, characteristics of a simple monopole antenna, which is mounted on an infinite ground plane [11–13] and excited by a compressed pulse, output of an axially symmetric compressor [1], are studied. These studies are carried out in two steps: (i) First, the characteristics of the monopole, namely the frequency-domain radiation efficiency and the power and pulse patterns, are obtained under a broadband excitation to observe all possible modes of operation clearly. The interesting features of the obtained characteristics are pointed out. (ii) The mount and geometry of the monopole are modified to match the output of the axially symmetric compressor from [1]. The characteristics of the modified monopole under the compressed pulse excitation are studied.

The remainder of this section is organized as follows: In Section 3.1, the characteristics of the monopole under a broadband

excitation are studied. In Section 3.2, the characteristics of the modified monopole excited by the output pulse of an axially symmetric compressor [1] are studied.

3.1. Simple Monopole as a Radiator

The geometry of the monopole mounted on an infinite ground plane is shown in Fig. 1; the antenna is simply the elongated inner conductor of a coaxial waveguide over an infinite flange. Its geometrical parameters are set as $a = 1\,\mathrm{m}$, $b = 0.3\,\mathrm{m}$, and $d = 1.57\,\mathrm{m}$. The virtual boundaries $\mathbf{L}_1$ and $\mathbf{L}_2$ are set at $z = -L_1 = -0.5\,\mathrm{m}$ and $r = L_2 = 8.0\,\mathrm{m}$, respectively. The electromagnetic wave interactions on this structure are described by the initial-boundary value problem (1) (see Section 2.1). To obtain the monopole's characteristics over a wide frequency range, the monopole is excited with a broadband pulse. As the output of the axially symmetric compressor is a $TM_{0,0}$ (TEM) mode pulse [1], the monopole is excited with the wideband pulse of the same type. This excitation is implemented by setting $v_{0,1}(-L_1, t) = 4\sin(\Delta k(t-\tilde{T}))\cos(\tilde{k}(t-\tilde{T}))(t-\tilde{T})^{-1}\chi(\bar{T}-t)$. Here, $v_{0,1}(-L_1, t)$ is the amplitude of the pulse on the virtual boundary $\mathbf{L}_1$ $(z = -L_1)$ (see (2)), $\chi(\cdot)$ is the Heaviside step function, and parameters $\bar{T}$, $\tilde{T}$, $\tilde{k}$, Δk, and the range $(\tilde{k} - \Delta k; \tilde{k} + \Delta k)$ are the duration, delay, the modulation (center) frequency, the bandwidth, and the frequency band of the pulse, respectively. These parameters are chosen as $\tilde{k} = 8\,\mathrm{rad/m}$, $\Delta k = 7.5$, $\tilde{T} = 30\,\mathrm{m}$, and $\bar{T} = 100\,\mathrm{m}$; this choice of parameters results in the pulse whose spectrum uniformly occupies the frequency band $0.5 \le k \le 15.5\,\mathrm{rad/m}$. Within this frequency range, the monopole exhibits the following behavior [11–13]:

The frequency-domain radiation efficiency, $\eta_{fr}(k)$, monotonically grows from zero to $\bar{\eta}_1 \approx 1$ within the frequency band $0 < k < \bar{K}_1$. The first local maximum $\bar{\eta}_1$ of $\eta_{fr}(k)$ occurs at $k = \bar{K}_1 = 1.1\,\mathrm{rad/m}$, which approximately corresponds to $\lambda = 4d$, the second local maximum $\bar{\eta}_2$ occurs at $k = \bar{K}_2 = 3.2\,\mathrm{rad/m}$, which approximately corresponds to $3\lambda = 4d$ (see Fig. 2(a)). It is clear that the maxima are associated with the quarter-wave resonances. The first local minimum $\underline{\eta}_1$ of $\eta_{fr}(k)$ occurs at $k = \underline{K}_1 = 2.0\,\mathrm{rad/m}$, which approximately corresponds to $\lambda = 2d$, the second local minimum $\underline{\eta}_2$ occurs at $k = \underline{K}_2 = 3.9\,\mathrm{rad/m}$, which approximately corresponds to $\lambda = d$ (see Fig. 2(a)). It is clear that the minima are associated with the half-wave resonances. For the frequencies $k > k_1 = 4.41\,\mathrm{rad/m}$ (k_1 is the cut-off frequency of $TM_{0,1}$ wave), the frequency-domain radiation efficiency $\eta_{fr}(k)$ is virtually one (see Fig. 2(a)).

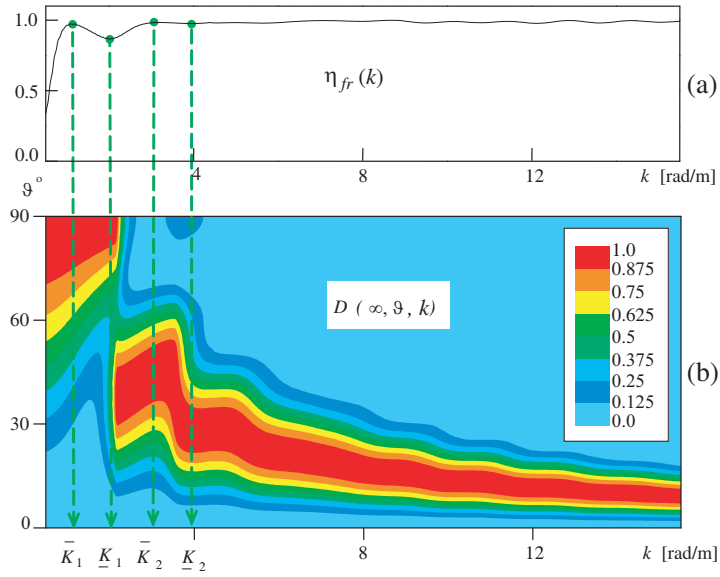

Figure 2. Characteristics of the monopole: (a) frequency-domain radiation efficiency; (b) far-field normalized power pattern.

For the frequencies $k > k_2 = 8.93\,\text{rad/m}$ (k_2 is the cut-off frequency of $TM_{0,2}$ wave), the normalized power pattern, $D(M, \vartheta, k)$, changes smoothly with increasing k, and its main lobe gradually gets narrow and finally reaches the direction of $\bar{\vartheta} < 10°$ (see Fig. 2(b)).

The normalized power pattern has abrupt changes in the vicinities of the frequencies $k = \underline{K}_n$; $n = 1, 2$: the main lobe gets much closer to the z axis and becomes narrower, and then smoothly turns back (see Fig. 2(b)). This means that a pulse could be strongly distorted if its central frequency coincides with any of the frequency points $\underline{K}_n$.

For $0 < k < \underline{K}_1$ (relatively low frequencies), the radiated waves propagate perpendicular to the axis of symmetry (z axis, see Figs. 2(b)). Hence, in this mode of operation, it is possible to use the monopole as a feeding element for planar structures or various antennas.

A pulse, whose spectral amplitudes are nonzero only for $k > k_1$, is radiated without forerunner pulse, and its low-amplitude tail cannot compete with the main pulse (see Fig. 3(a)). The time-domain radiation efficiency ξ is higher than 0.97. The radiated signal is well-focused and propagates in the direction $\bar{\vartheta}$ which is determined by the central frequency of the pulse $\tilde{k}$: larger $\tilde{k}$ corresponds to smaller $\bar{\vartheta}$ (see Figs. 3(a) and (b)).

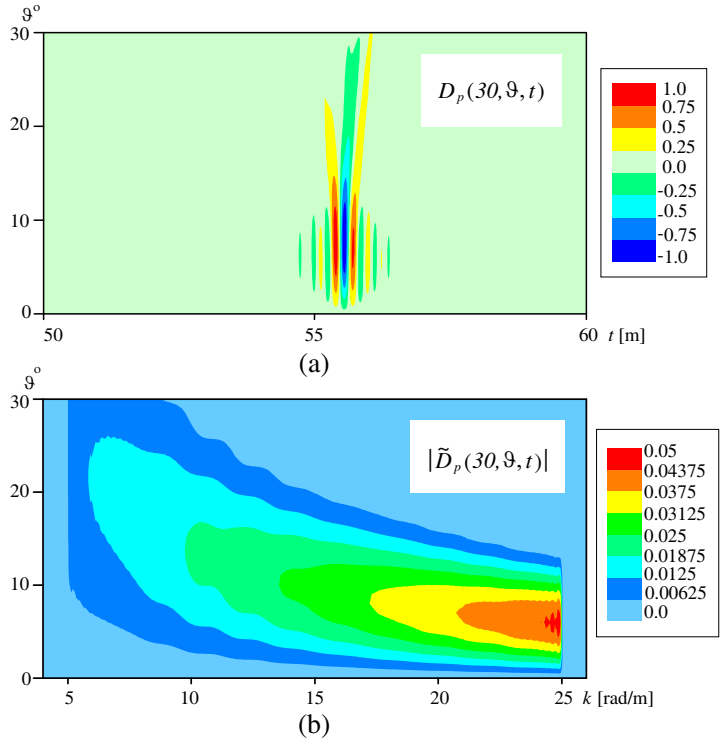

Figure 3. (a) Normalized pulse pattern of the monopole on the arc $r = M = 30\,\text{m}$. (b) Its Fourier transform.

Part of the information and observations presented above might be considered as expected or known, but when assembled together, they provide a rather full insight on the physics and mechanics of the radiation from monopole antennas.

3.2. Radiation of a Compressed Pulse by a Monopole

A monopole antenna mounted on a infinite ground plane is excited by the output of the axially symmetric microwave compressor that was designed in [1]. It should be recalled here that the output pulse of this compressors is a short high-power TEM pulse $U(g,t) = u_{0,2}(L_4,t)\mu_{0,2}(\rho)$, which was exhausted into the coaxial output waveguide. Here, $u_{0,2}(L_4,t)$ and $\mu_{0,2}(\rho)$ are the mode amplitude of the output pulse and the coaxial waveguide's transverse function (see (2)). The central frequency of this pulse is $\tilde{k} = 2.723\,\text{rad/m}$, its bandwidth

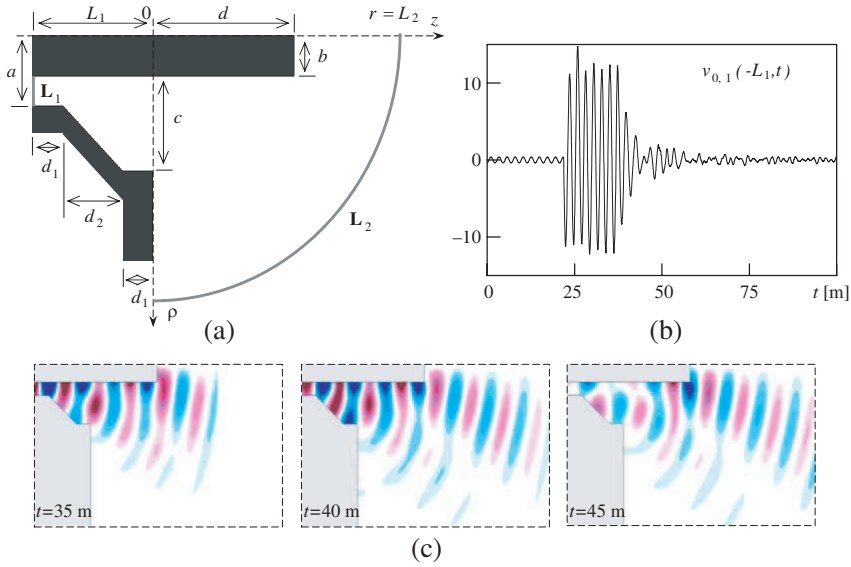

Figure 4. (a) Geometry of the modified monopole. (b) Time signature of the compressed pulse. (c) Field pattern of H_ϕ component.

is around $2.5 \leq k \leq 2.9\,\text{rad/m}$, and its length is $T_2^s \approx 4023 - 4002 = 21\,\text{m}$ [1]. The radii of the coaxial waveguide's inner and outer conductors are 0.9 m and 1.56 m, respectively. The modified monopole antenna is designed from the simple monopole studied in Section 3.1 (see Fig. 4(a)). The feeding waveguide of this antenna matches with the coaxial output waveguide of the compressor ($a = 1.56\,\text{m}$, $b = 0.9\,\text{m}$). The radius of the inner conductor (i.e, the radius of the monopole itself) is tripled to make it match the inner conductor of the antenna's feeding waveguide, $c + b = 3.0\,\text{m}$, $d = 4.71\,\text{m}$), the opening of the feeding waveguide is smoothly widen to make the waveguide's outer conductor match to that of the radiating end ($d_1 = 1.0\,\text{m}$, $d_2 = 2.0\,\text{m}$, $L_1 = 2d_1 + d_2$). The modified monopole antenna is excited with the compressed pulse: $v_{0,1}(-L_1, t) = u_{0,2}(L_4, t + 3980)$, its time signature is presented in Fig. 4(b).

Taking into account the central frequency of the compressed pulse ($\tilde{k} = 2.723\,\text{rad/m}$) and studying the data associated with the band $3\tilde{k} \pm 0.7 \approx 8.17 \pm 0.7\,\text{rad/m}$ in Figs. 2 and 3 (the three-fold scaling of frequency is caused by the scaling of monopole), it is possible to state confidently that the efficiency and the directivity of radiation of the modified monopole will be rather high. The simulation results fully confirm this statement (see Figs. 4(c) and 5): the time-domain

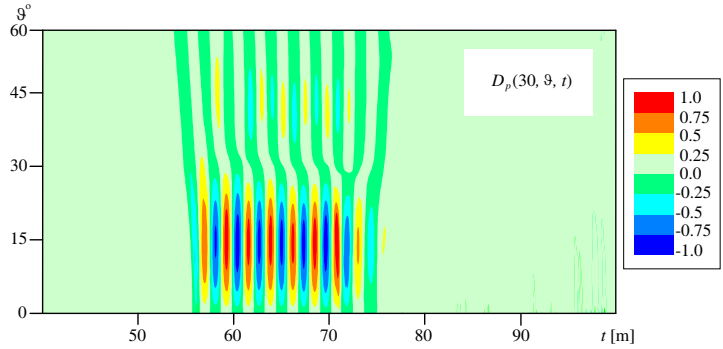

Figure 5. Radiation of the compressed pulse by the modified monopole: normalized pulse pattern on the arc $r = M = 30\,\mathrm{m}$.

radiation efficiency is $\xi = 0.981$, the frequency-domain radiation efficiency varies from $\eta_{fr} = 0.965$ (at $k = 2.87\,\mathrm{rad/m}$ to $\eta_{fr} = 0.999$ (at $k = 2.6\,\mathrm{rad/m}$, the direction of the main lobe of the pulsed pattern is $\bar{\vartheta}_P \approx 15^\circ$ and the HPBW of this lobe is $\vartheta_P^{0.5} \approx 13^\circ$ (see Fig. 5). The weak side lobe ($\vartheta \approx 45^\circ$, Fig. 5) is caused by the undamped $TM_{0,1}$ mode of the wide coaxial waveguide, which propagates and radiates when $k > 1.47\,\mathrm{rad/m}$.

Even though the results presented in this section show that a monopole antenna might be used efficiently for radiating short pulses, depending on the specifications of the application at hand, more complex antennas or antenna arrays might be needed. More directive radiation patterns can be obtained using advanced antennas such as horn or reflector antennas, or arrays constructed using those [12–14, 17, 25]. In the next section, radiation of compressed pulses from phased antenna arrays is studied and a new design, where each of the array elements is constructed by combining a radiator and a microwave compressor, is proposed.

4. COMPRESSION AND BEAMED RADIATION OF PULSES BY A NEW ARRAY DESIGN

This section presents a novel array design, where each of the array elements is constructed by combining a microwave compressor and a radiator. The proposed design has several advantages over the "common" array designs: (i) The overall size and the weight of the array is reduced since the waveguide between the compressor and the radiator is now removed. (ii) The pulse distortion and the absorption loss are reduced since the overall distance covered by pulse in lossy

and dispersive waveguides is decreased. (iii) The pulse is compressed right before it is radiated; this allows for the use of devices that cannot handle high power in the rest of the array. Additionally, losses encountered in the rest of the array can be compensated by simply increasing the duration of compression applied before the radiation.

In this work, this novel design idea is applied to a phased antenna array. It would be correct to say that this paper for the first time demonstrates the possibility of such a design on the elements of a phased antenna array. This is done in three steps: (i) The "common" phased array is designed and its radiation characteristics are studied. (ii) The novel antenna elements are designed by combining a microwave compressor and the radiating elements of the phased array in step (i). (iii) The combined compressor/radiator elements are assembled together to construct an improved phased array.

The improved phased array is intended for beamed radiation of high-power short pulses; the new design shares the advantages of "common" phased arrays in addition to the advantages listed above. The proposed design can serve in radar systems, where rapid steering of the antenna's main beam is essential, or in antenna systems for airborne and space vehicles, where it is beneficial to eliminate the antenna's mechanical steering drive for reduced size and weight and increased reliability and life time.

In this work, it is assumed that the radiator and the compressor units are constructed using rectangular waveguides, and the feeding waveguides are excited by $TE_{0,n}$ waves ($E_y = E_z = H_x = 0$). Under this assumption, since there is no field variation in the x direction, the devices under study are accurately modelled using the 2-D structure in the $y0z$ plane (Fig. 6). The electromagnetic wave interactions on such structures are described by the initial-boundary value problem (3.21) in [17]. It should be noted here that, for more general cases and more complicated structures, three-dimensional (3-D) models are needed to accurately model the pertinent physics. In such cases, only the electromagnetic initial-boundary value problem will be different; however, the discussions on the operation principles and characteristics presented here would be unchanged.

The remainder of this section is organized as follows: In Section 4.1, characteristics of the "prototype" phased array and its radiating elements are outlined. In Section 4.2, the new array elements each of which integrates a microwave compressor and a radiator unit are designed. The characterization of this new array element is done. Section 4.3, studies the characteristics of a phased array constructed assembling 13 of these new combined antenna elements.

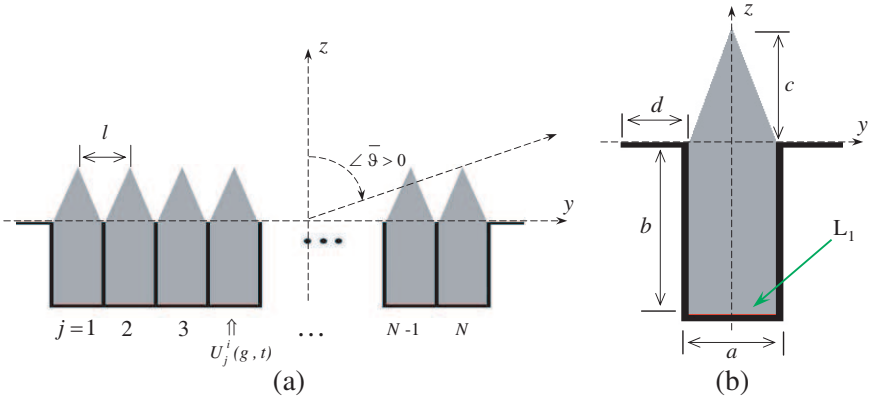

Figure 6. (a) Geometry of the 2-D phased array. (b) Geometry of a single array's element.

4.1. Phased Array as a Radiator

The prototype of the radiating antenna is the 2-D phased array, which was designed in [25]. The array consists of 13 identical radiating elements, which are arranged along the y axis with the period $l = 0.014\,\text{m}$ (Fig. 6(a)). Each of the radiating elements is a flanged open end of PEC rectangular waveguide filled with dielectric ($\varepsilon_r = 2.5$), which projects out of the waveguide and has a triangular shape (Fig. 6(b)). Its dimensions are set as $a = 0.0132\,\text{m}$, $b = L_1 = 0.03\,\text{m}$, $c = 0.02\,\text{m}$, $d = 0.01\,\text{m}$, and the thickness of the PEC walls is $0.0008\,\text{m}$ (Fig. 6(b)). It should be noted here that when assembled into the array, only the first and the last radiating element retain their left and right flanges, respectively. The array is excited by $TE_{0,1}$ waves. The frequency domain efficiency of the array, $\eta_{fr,arr}(k)$, is never less than 0.9 within the band $168 \le k \le 251\,\text{rad/m}$ for scanning angle $-45^\circ \le \bar{\vartheta} \le 45^\circ$ (the band $168 \le k \le 251\,\text{rad/m}$ corresponds to the frequency band $8 \le f \le 12\,\text{GHz}$). The HPBW of the major lobe varies from $\vartheta_{0.5}(k) = 7.0^\circ$ ($k = 251\,\text{rad/m}$ and $\bar{\vartheta} = 0^\circ$) to $\vartheta_{0.5}(k) = 13.9^\circ$ ($k = 168\,\text{rad/m}$ and $\bar{\vartheta} = \pm 45^\circ$). The direction of the main beam is set by the relative delay of the excitation of each radiating element, $\Delta t = \sin(\bar{\vartheta})l$ (if the first radiating element is excited by the wave $U_1^i(y,z,t)$ then the second one is excited by the wave $U_2^i(y,z,t) = U_1^i(y-l,z,t+\Delta t)$ and so on) [26]. For example, $\bar{\vartheta}(k) = 15^\circ$ for $\Delta t = \sin(15^\circ)l \approx 0.36\,\text{m}$, $\bar{\vartheta}(k) = 30^\circ$ for $\Delta t = \sin(30^\circ)l \approx 0.7\,\text{m}$, and $\bar{\vartheta}(k) = 45^\circ$ for $\Delta t = \sin(45^\circ)l \approx 0.99\,\text{m}$. It should be noted here that despite the presence of the PEC wall

at the bottom of elements (Fig. 6), the infinite feeding waveguides are simulated using the concept of virtual feeding waveguide, which is presented in [15].

4.2. Combined Compressor/Radiator Array Elements

The compressor similar to one designed and studied in Part I is used as the prototype of the compressor unit to be combined with the radiator to generate the compressor/radiator array element. To allow for the integration of the compressor with the feeding waveguide of the radiator, the geometrical parameters of the combined array element are set as $a = 0.0132\,\text{m}$, $b = 0.036\,\text{m}$, $c = 0.02\,\text{m}$, $d = 0.01\,\text{m}$ and $L_1 = 0.048\,\text{m}$ (Fig. 7(a)). The thickness of the PEC walls is 0.0008 m. The storage unit has the same width, a, as the feeding waveguide, and they are coupled via thin beyond-cutoff diaphragm [27–29]. The size of the coupling window is 0.0028 m and the thickness of diaphragm is 0.0004 m. In the frequency band of interest, $168 \leq k \leq 251\,\text{rad/m}$, the feeding waveguide and the storage unit support only one $TE_{0,1}$ mode. The switch similar to the one designed in Part I is used (Fig. 7(a)). During the energy accumulation, the switch is locked and

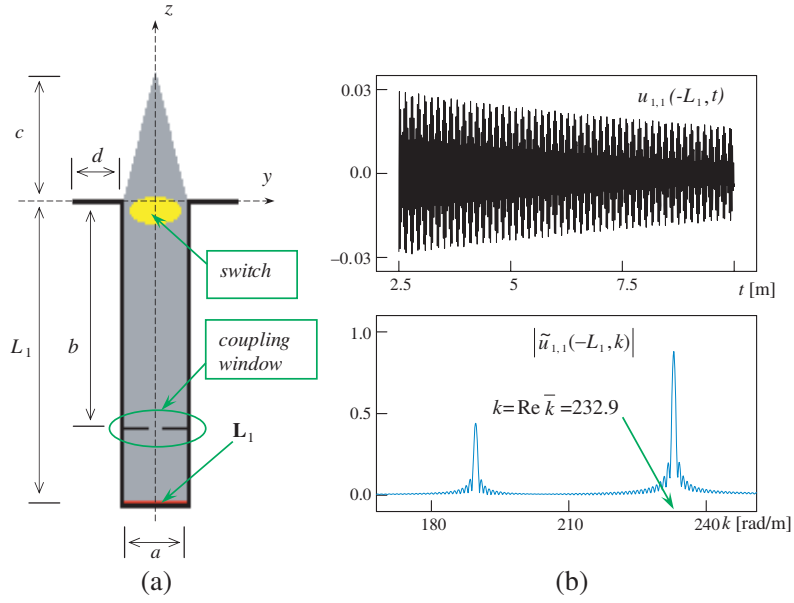

Figure 7. (a) Geometry of the compressor/radiator array's element. (b) Excitation of the array's element by a broadband pulse.

$\sigma_0 = 5.7 \cdot 10^4$ S/m inside the switch, during the exhaust of accumulated energy the switch is unlocked and $\sigma_0 = 0$ inside the switch.

As it is explained in the compressors' design scheme (see [1] and Part I of this paper), to determine the eigenfrequencies of the storage unit, the compressor/radiator array element with locked switch is excited with the broadband Gaussian $TE_{0,1}$ pulse: $v_{1,1}(0,t) = F_1(t) = \exp[-(t-\tilde{T})^2 \Big/ 4\alpha^2] \cos[\tilde{k}(t-\tilde{T})]\chi(\bar{T}-t)$. Here, the parameters $\bar{T}$, $\tilde{T}$, $\tilde{k}$, and α represent the duration, delay, modulation (center) frequency, and the bandwidth of the pulse, respectively. These parameters are chosen as $\bar{T} = 0.3$ m, $\tilde{T} = 0.15$ m, $\tilde{k} = 200$ rad/m, and $\alpha = 0.02$. As the feeding waveguide and the storage unit support only one $TE_{0,1}$ mode, it is possible to get the eigenfrequencies of the storage unit by studying the spectrum of the reflected wave after the shutdown of excitation. Indeed, the non-resonant frequencies dissipate soon after the end of excitation, and it is free-oscillating resonant eigenfrequencies which contribute to the spectrum of the reflected wave after the end of excitation. Thus, the peaks in normalized spectrum of the reflected wave after the end of excitation clearly identify the real parts $\mathrm{Re}\bar{k}$ of complex eigenfrequencies $\bar{k}$ (Fig. 7(b)). This normalized spectrum is obtained by Fourier transforming the spatio-temporal amplitude of free-oscillating (in the absence of the excitation) field, $u_{1,1}(-L_1,t)$, $t > \bar{T}$, (this operation provides spectral amplitude $\tilde{u}_{1,1}(-L_1,k)$), and subsequently dividing the spectral amplitude $\tilde{u}_{1,1}(-L_1,k)$ by the Fourier transform of the excitation's time signature, $\tilde{F}_1(k)$. The eigenfrequency $\mathrm{Re}\bar{k} = 232.9$ corresponds to the high-Q eigenoscillation of the storage unit (Fig. 7(b)), so this frequency is chosen as the working frequency for the combined compressor/radiator element, $k_{work} = 232.9$ rad/m (see Part I for details of the working frequency choice).

The Q-factor of the working oscillation is obtained by exciting the combined compressor/radiator element with the narrowband Gaussian pulse with the central frequency $\tilde{k} = k_{work} = 232.9$ rad/m: $v_{1,1}(0,t) = F_1(t)$, with $\bar{T} = 2$ m, $\tilde{T} = 1$ m and $\alpha = 0.2$, and studying the behavior of free oscillating field $U(g,t)$ in the antinodal point g_1 (see Fig. 8(b), the antinodal point $g_1 = \{y = 0.0,\ z = -0.009\}$ is marked in Fig. 8(a)). The amplitude of free-oscillating field $U(g_1,t)$ decreases with time t as $\exp(-t|\mathrm{Im}\bar{k}|)$, so the value of $|\mathrm{Im}\bar{k}|$ and, thus the Q-factor, can be found (see [30–32] for methodology). For the combined compressor/radiator element considered here, $\mathrm{Im}\bar{k} = -0.095$ and the Q-factor (see (13) in Part I) is $Q \approx 1225.8$. For the sake of completeness, it should be noted here that the type of working oscillation is $TE_{0,1,3}$ (Fig. 8(a)).

The energy accumulation characteristics of the compres-

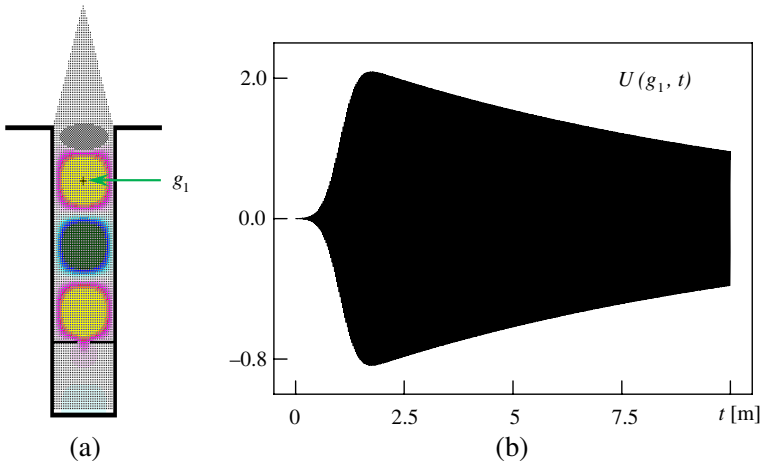

Figure 8. Excitation of the compressor/radiator element by the narrowband Gaussian pulse: (a) Field pattern (E_x component) at the instant of time $t = 2.5\,\mathrm{m}$ (free oscillations); (b) Amplitude of the field (E_x component) at the antinodal point g_1.

sor/radiator array element are obtained by exciting it with the long quasi-monochromatic pulse: $v_{1,1}(0,t) = F_2(t) = Tr(t)\cos(\tilde{k}t)$. Here, $Tr(t)$ represents a trapezoidal envelope which is equal to zero for $t < t_{start}$ and $t > t_{end}$, and is equal to one for $t_{oneL} < t < t_{oneR}$. The parameters of excitation are chosen as $\tilde{k} = k_{work} = 232.9\,\mathrm{rad/m}$, $t_{start} = 0.001\,\mathrm{m}$, $t_{oneL} = 0.05\,\mathrm{m}$, $t_{oneR} = 40\,\mathrm{m}$, $t_{end} = 40.05\,\mathrm{m}$. Fig. 9 plots the instantaneous power of the excitation and the reflected wave, and the field intensity in the antinodal point g_1; Table 1 shows the values of the instantaneous energy accumulation efficiency $\eta_{accum}(t)$ (see its definition in (8) in Part I), the normalized field intensity of working oscillation in antinodal point $\alpha(t) = \max\limits_{0<\tau\leq t} |U(g_1,\tau)| / \max\limits_{\tau>0} |U(g_1,\tau)|$ and the power gain at the distinguished instants of time: around $t = 7.5\,\mathrm{m}$ there is almost no reflection back into the feeding waveguide (Fig. 9(b)); between $t = 15\,\mathrm{m}$ and $t = 22.5\,\mathrm{m}$ the function $\eta_{accum}(t)$ reaches its maximum; $t = 30\,\mathrm{m}$ is a midpoint between maximum efficiency and maximum field intensity; around $t = 40\,\mathrm{m}$ the function $\alpha(t)$ reaches it maximum, hence, the amplitude of the field inside the storage unit does not grow any more (Fig. 9(c)). The excitation's duration $T^i = 29.95\,\mathrm{m}$ is chosen as a good tradeoff between the amplitude of compressed pulse and the efficiency (see discussion of the selection of the excitation's duration in Section 3.3.3 of Part I).

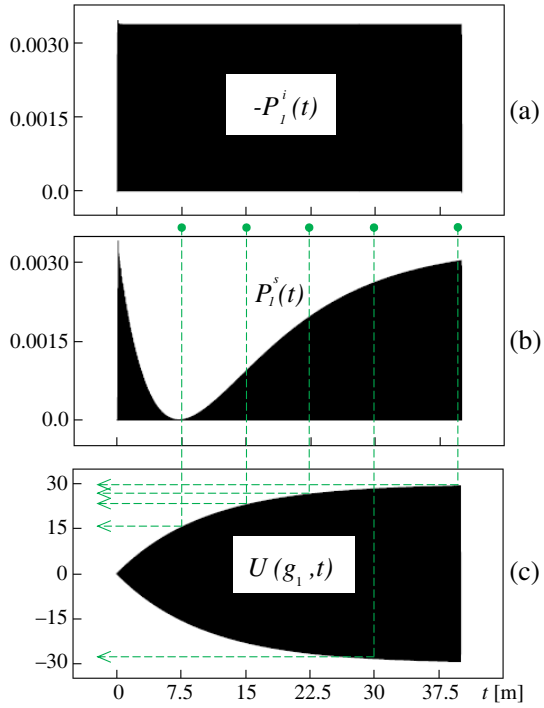

Figure 9. Accumulation of the energy: (a) Instantaneous power of the excitation; (b) Instantaneous power of the wave reflected back into the feeding waveguide; (c) Electric field (E_x component) intensity in the antinodal point g_1.

Table 1. Energy accumulation efficiency, normalized field intensity and power gain at the distinguished instants of time.

	$t = 7.5$ m	15 m	22.5 m	30 m	40 m
$\eta_{accum}(t)$	0.74	0.81	0.72	0.61	0.49
$\alpha(t)$	0.52	0.78	0.90	0.96	0.99
$\theta(t)$ for $T^i = t$	37	81	107	122	128

An interesting observation can be made by comparing Fig. 9 and Table 1 of this paper with Fig. 7 and Table 1 of Part I: the compressors under study exhibit qualitatively similar behavior despite all the differences in the compressor's geometry, the type and frequency of working oscillations and the Q-factors.

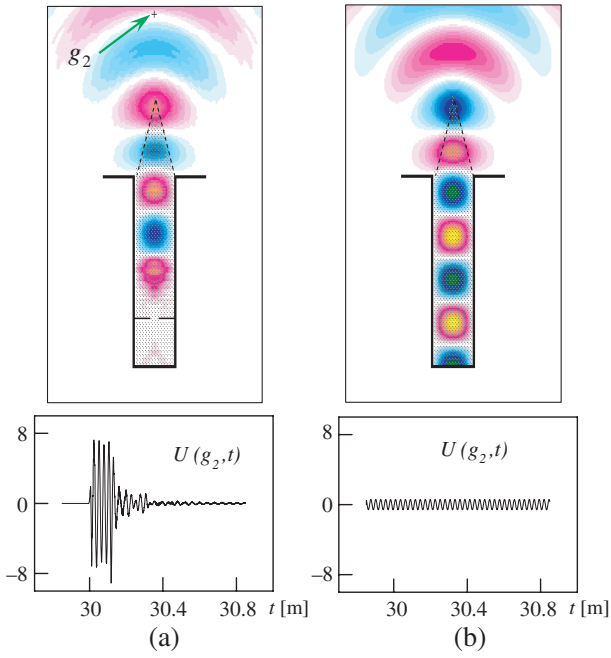

Figure 10. Radiation of (a) short compressed pulse, and (b) long un-compressed pulse. Field patterns (E_x component) are shown at the instant of time $t = 30.03$ m.

When the duration of excitation is set ($T^i = 29.95$ m), the switch operates as following: until the instant of time $t = 29.94$ m it is locked, and starting from $t = 29.95$ m it is open. On the short time interval $29.94 \leq t \leq 29.95$ m the specific conductivity of the medium inside the switch changes from $\sigma_0 = 5.7 \cdot 10^4$ S/m down to $\sigma_0 = 0$. The whole compressor/radiator array element operates as following: during the energy accumulation ($0 < t < 29.95$ m) it is excited with the long quasi-monochromatic pulse $U^i(g,t)$: $v_{1,1}(0,t) = F_2(t)$ with $\tilde{k} = k_{work} = 232.9$ rad/m, $t_{start} = 0.001$ m, $t_{oneL} = 0.05$ m, $t_{oneR} = 29.95$ m, $t_{end} = 29.99$ m. At time $t = T^i = 29.95$ m the excitation is turned off, the switch opens and a high-power short RF pulse is radiated into the free space. The radiated pulse passes by the observation point $g_2 = \{y = 0, z = 0.027\}$ during the time $T_2^s = 30.15 - 30 = 0.15$ m (Fig. 10(a)). In the observation point g_2, the amplitude of compressed pulse is roughly 13 times higher than the amplitude of excitation pulse (Fig. 10). The compressor characteristics of the array element are computed using the definitions in Section 2

of Part I: the energy efficiency $\eta = 0.608$, the degree of compression $\beta = T^i/T_2^s \approx 199.7$, the power gain $\theta = \beta \cdot \eta = 121.4$. The efficiency η is a bit smaller than the efficiency of energy accumulation $\eta_{accum}(T^i)$ because a fraction of the accumulated energy goes into the tail following the main output pulse (see $U(g_2, t)$ for $t \geq 30.15\,\mathrm{m}$ in Fig. 10(a)).

4.3. Phased Array Assembled Using Compressor/Radiator Elements

To construct a phased array of the combined compressor/radiator elements, 13 of them are assembled with period $l = 0.014\,\mathrm{m}$ (see Fig. 11(a)). Similar to the common phased array design presented in [25], when assembled into the array, only the first and the last elements retain their left and right flanges, respectively. The array is excited using the method described next: The first array element is excited with the long quasi-monochromatic pulse $U_1^i(y, z, t) = U^i(y, z, t)$: $v_{1,1}(0, t) = F_2(t)$ with $\tilde{k} = k_{work} = 232.9\,\mathrm{rad/m}$, $t_{start} = 0.001\,\mathrm{m}$, $t_{oneL} = 0.05\,\mathrm{m}$, $t_{oneR} = 29.95\,\mathrm{m}$, $t_{end} = 29.99\,\mathrm{m}$. The second array element is excited with the same pulse delayed by Δt: $U_2^i(y, z, t) = U_1^i(y - l, z, t + \Delta t)$. The third one is excited with $U_3^i(y, z, t) = U_2^i(y - l, z, t + \Delta t)$ and so on. Here, Δt represents the delay and it is defined as $\Delta t = \sin(\bar{\vartheta})l$; this delay is set by the desired direction of the main beam $\bar{\vartheta}$, $-45^\circ \leq \bar{\vartheta} \leq 45^\circ$ [26], see also Section 4.1 and Fig. 6(a). The switch of the first array element opens at time $t = t_1 = 29.95\,\mathrm{m}$, the switch of the second element opens at $t_2 = t_1 + \Delta t$ and so on. Thus, the energy accumulation in each array element lasts for the same amount of time, and the lengths of pulses compressed in each element are also the same.

Figure 11 presents the results of simulation of the compression and radiation of short high-power RF pulse by the compact phased array. The delay for this simulation is set as $\Delta t = \sin(30^\circ)l = 0.007\,\mathrm{m}$. The direction of the main beam perfectly coincides with the expected one: $\bar{\vartheta} = 30^\circ$ for $\Delta t = \sin(30^\circ)l$ (Fig. 11(a)). With variation of the delay within $0 \leq |\Delta t| \leq 0.0099\,\mathrm{m}$, the direction of the main beam changes within $-45^\circ \leq \bar{\vartheta} \leq 45^\circ$. The directivity of radiation is very high: for $\bar{\vartheta} = 30^\circ$ the HPBW (see its definition in Section 2.2) is non-greater than $\vartheta_{0.5} = 8.3^\circ$ (Fig. 11(c)). The amplitude of the pulse with flat edge, which is compressed and radiated by the array, is slightly higher than the amplitude of the pulse radiated by the single array element (compare Fig. 11(b) and Fig. 10(a)).

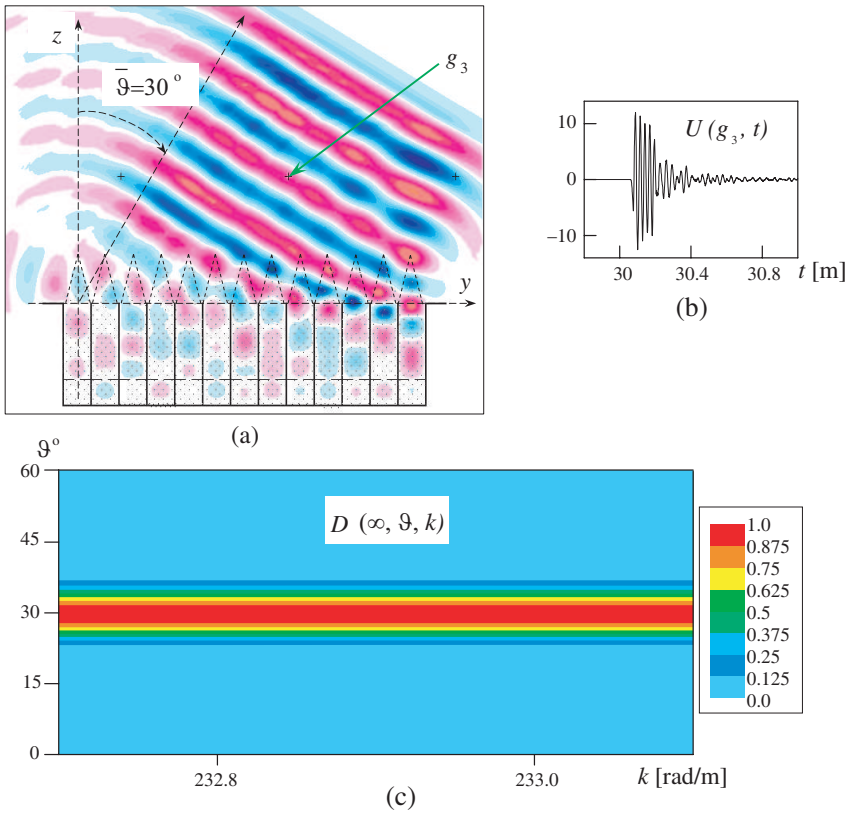

Figure 11. Compression and radiation of a short pulse by the array of 13 elements. (a) Field pattern (E_x component) at the instant of time $t = 30.14$ m. (b) Amplitude of the radiated pulse at the point g_3 in the near-field zone of the phased array. (c) The normalized power pattern.

5. CONCLUSIONS

The paper, first, studies the radiation of a short RF pulse from a monopole antenna mounted on a ground plane. With this study, it is demonstrated that the compressed pulses can efficiently be radiated using simple antennas. Then, a novel array design, where each of the array elements is constructed by combining a compressor and a radiator, is presented. The new design allows to reduce the overall size and the weight of the array, distortion in the pulse and the absorption loss. Additionally, the proposed design has the advantage of compressing the pulse right before it is radiated, allowing the use of

devices that cannot handle high power in the rest of the array. This design idea is applied to a phased antenna array; the improved phased antenna array is intended for generation and directional radiation of high-power short pulses and shares the most significant advantage of "common" phased arrays, viz. rapid electronic beam steering without the movement of the array itself.

REFERENCES

1. Kuzmitchev, I. K., P. M. Melezhyk, V. L. Pazynin, K. Y. Sirenko, Y. K. Sirenko, O. S. Shafalyuk, and L. G. Velychko, "Model synthesis of energy compressors," *Radiophysics and Electronics: Sci. Works Collection*, Vol. 13, No. 2, 166–172, 2008.
2. Vikharev, A. L., A. M. Gorbachev, O. A. Ivanov, V. A. Isaev, S. V. Kuzikov, B. Z. Movshevich, J. Hirshfield, and S. H. Gold, "Active Bragg compressor of 3-cm wavelength microwave pulses," *Radiophys. Quantum Electron.*, Vol. 51, No. 7, 539–555, 2008.
3. Andreev, A. D., E. G. Farr, and E. Schamiloglu, "A simplified theory of microwave pulse compression," *Circuit and Electromagnetic System Design Notes*, No. 57, 2008.
4. Tamura, F. and S. G. Tantawi, "Development of high power X-band semiconductor microwave switch for pulse compression systems of future linear colliders," *Phys. Rev. Spec. Top. Accel. Beams*, Vol. 5, 062001, 2002.
5. Faillon, G. and A.-J. Durand, "Microwave pulse generator incorporating a pulse compressor," U.S. Patent 6768266, July 27, 2004.
6. Artemenko, S. N., "Formation of nanosecond RF pulses in an autogenerator by resonance compression of microwave energy," *Radiophys. Quantum Electron.*, Vol. 41, No. 7, 616–624, 1998.
7. Bossart, R., P. Brown, J. Mourier, I. V. Syratchev, and L. Tanner, "High-power microwave pulse compression of klystrons by phase-modulation of high-Q storage cavities," *CERN CLIC-Notes*, No. 592, 2004.
8. Farr, E. G., L. H. Bowen, W. D. Prather, and C. E. Baum, "Microwave pulse compression experiments at low and high power," *Circuit and Electromagnetic System Design Notes*, No. 63, 2010.
9. Benford, J., "Space applications of high-power microwaves," *IEEE Trans. Plasma Sci.*, Vol. 36, No. 3, 569–581, 2008.
10. Giri, D. V., F. M. Tesche, and C. E. Baum, "An overview of high-power electromagnetics (HPEM) radiating and conducting

systems," *Circuit and Electromagnetic System Design Notes*, No. 50, 2006.

11. Sirenko, K., "Axially-symmetrical radiators of pulsed TM_{0n}- and TE_{0n}-waves," *Proc. MMET'06*, 321–323, 2006.
12. Sirenko, K. Y. and V. L. Pazynin, "Axially-symmetrical radiators of pulsed and monochromatic TE- and TM-waves," *Uspekhi Sovremennoi Radioelektroniki*, No. 4, 52–69, 2006 (in Russian).
13. Sirenko, K. Y., "Slot resonances in axially symmetric radiators of pulse-modulated and monochromatic TM_{0n}-modes," *Telecommunications and Radio Engineering*, Vol. 66, No. 1, 9–21, 2007.
14. Balanis, C. A., *Antenna Theory. Analysis and Design*, Wiley, New York, 2005.
15. Sirenko, K., V. Pazynin, Y. K. Sirenko, and H. Bagci, "An FFT-accelerated FDTD scheme with exact absorbing conditions for characterizing axially symmetric resonant structures," *Progress In Electromagnetics Research*, Vol. 111, 331–364, 2011.
16. Sirenko, K. Y. and Y. K. Sirenko, "Exact absorbing conditions in the initial boundary-value problems of the theory of open waveguide resonators," *Comput. Math. Math. Phys.*, Vol. 45, No. 3, 490–506, 2005.
17. Sirenko, Y. K., S. Strom, and N. P. Yashina, *Modeling and Analysis of Transient Processes in Open Resonant Structures. New Methods and Techniques*, Springer, Berlin, 2007.
18. Hairer, E., C. H. Lubich, and M. Schlichte, "Fast numerical solution of nonlinear Volterra convolution equations," *SIAM J. Sci. Stat. Comput.*, Vol. 6, No. 3, 532–541, 1985.
19. Yilmaz, A. E., D. S. Weile, B. Shanker, J.-M. Jin, and E. Michielssen, "Fast analysis of transient scattering in lossy media," *IEEE Antennas Wireless Propagat. Lett.*, Vol. 1, No. 1, 14–17, 2002.
20. Bagci, H., A. E. Yilmaz, and E. Michielssen, "A fast hybrid TDIE-FDTD-MNA scheme for analyzing cable-induced transient coupling into shielding enclosures," *Proc. IEEE Int. Symp. Electromagn. Compat.*, Vol. 3, 828–833, 2005.
21. Bagci, H., A. E. Yilmaz, V. Lomakin, and E. Michielssen, "Fast solution of mixed-potential time-domain integral equations for half-space environments," *IEEE Trans. Geosci. Remote Sensing*, Vol. 43, No. 2, 269–279, 2005.
22. Bagci, H., A. E. Yilmaz, and E. Michielssen, "FFT-accelerated MOT-based solution of time-domain BLT equations," *Proc. IEEE Int. Antennas Propagat. Symp.*, 1175–1178, 2006.

23. Bagci, H., A. E. Yilmaz, J.-M. Jin, and E. Michielssen, "Fast and rigorous analysis of EMC/EMI phenomena on electrically large and complex structures loaded with coaxial cables," *IEEE Trans. Electromagn. Compat.*, Vol. 49, No. 2, 361–381, 2007.
24. Bagci, H., A. E. Yilmaz, and E. Michielssen, "An FFT-accelerated time-domain multiconductor transmission line simulator," *IEEE Trans. Electromagn. Compat.*, Vol. 52, No. 1, 199–214, 2010.
25. Sirenko, Y. K. and S. Strom, Eds., *Modern Theory of Gratings. Resonant Scattering: Analysis Techniques and Phenomena*, Springer, Berlin, 2010.
26. Bhattacharyya, A., *Phased Array Antennas and Subsystems: Floquet Analysis, Synthesis, BFNs, and Active Array Systems*, John Wiley & Sons, New York, 2006.
27. Shestopalov, V. P., A. A. Kirilenko, and L. A. Rud', "Waveguide discontinuities," *Resonance Wave Scattering*, Vol. 2, Naukova Dumka, Kiev, 1986 (in Russian).
28. Pozar, D. M., *Microwave Engineering*, Wiley, New York, 1998.
29. Belous, O. I., A. A. Kirilenko, V. I. Tkachenko, A. I. Fisun, and A. M. Fursov, "Excitation of an open stripline resonator by a plane waveguide," *Radiophys. Quantum Electron.*, Vol. 37, No. 3, 181–189, 1994.
30. Sirenko, Y. K., L. G. Velychko, and F. Erden, "Time-domain and frequency-domain methods combined in the study of open resonance structures of complex geometry," *Progress In Electromagnetics Research*, Vol. 44, 57–79, 2004.
31. Velychko, L. G., Y. K. Sirenko, and O. S. Shafalyuk, "Time-domain analysis of open resonators. Analytical grounds," *Progress In Electromagnetics Research*, Vol. 61, 1–26, 2006.
32. Velychko, L. G. and Y. K. Sirenko, "Controlled changes in spectra of open quasi-optical resonators," *Progress In Electromagnetics Research B*, Vol. 16, 85–105, 2009.